

Modeling the electronic structures of the ground and excited states of the ytterbium atom and the ytterbium dimer: A modern quantum chemistry perspective.

Paweł Tecmer*, Katharina Boguslawski[†]*, Mateusz Borkowski*,
Piotr Szymon Żuchowski*, and Dariusz Kędziera[†]

May 1, 2019

Abstract

We present a comprehensive theoretical study of the electronic structures of the Yb atom and the Yb₂ molecule, respectively, focusing on their ground and lowest-lying electronically excited states. Our study includes various state-of-the-art quantum chemistry methods such as CCSD, CCSD(T), CASPT2 (including spin-orbit coupling), and EOM-CCSD as well as some recently developed pCCD-based approaches and their extensions to target excited states. Specifically, we scan the lowest-lying potential energy surfaces of the Yb₂ dimer and provide a reliable benchmark set of spectroscopic parameters including optimal bond lengths, vibrational frequencies, potential energy depths, and adiabatic excitation energies. Our in-depth analysis unravels the complex nature of the electronic spectrum of Yb₂, which is difficult to model accurately by any conventional quantum chemistry method. Finally, we scrutinize the bi-excited character of the first $^1\Sigma_g^+$ excited state and its evolution along the potential energy surface.

*Institute of Physics, Faculty of Physics, Astronomy and Informatics, Nicolaus Copernicus University in Torun, Grudziadzka 5, 87-100 Torun, Poland; email: ptecmer@fizyka.umk.pl

[†]Department of Chemistry, Nicolaus Copernicus University in Torun, Gagarina 7, 87-100 Torun, Poland

INTRODUCTION

The divalent ytterbium atom has in recent years garnered significant attention thanks to its many uses in cold atom physics. It has a non-magnetic 1S_0 ground state and several useful optical transitions: the strong $^1S_0 \leftrightarrow ^1P_1$ line can be used for Zeeman slowing, whereas the narrow (181 kHz) intercombination $^1S_0 \leftrightarrow ^3P_1$ line can be used to directly laser cool Yb atoms to microkelvin temperatures¹. Yb has seven stable isotopes: two fermions (171 and 173 with nuclear spins of 1/2 and 5/2, respectively) and five bosons (168, 170, 172, 174, and 176) that lack nuclear spin. The rich isotope structure makes it possible to mass-tune the atomic interactions² and facilitates a wide array of possible quantum-degenerate gases^{3–6}. The doubly forbidden $^1S_0 \leftrightarrow ^3P_0$ transition lies at the heart of optical atomic clocks⁷ which are among the most precise physical instruments known to mankind. For example, an ytterbium clock has recently been demonstrated to enable geopotential measurements with an accuracy below a centimetre⁸. The long lived 3P_0 clock states also find use in quantum simulations using Yb atoms⁹.

The long range interactions in the Yb dimer have been probed extensively by high resolution photoassociation spectroscopy (PAS)¹⁰ near the narrow $^1S_0 \leftrightarrow ^3P_1$ intercombination line. The excited $^1S_0 + ^3P_1$ (0_u^+)^{11,12} state has been probed by single color PAS and provided the van der Waals C_6 coefficient and an improved value of the atomic 3P_1 lifetime. Two-color PAS of ground state 0_g^+ vibrational levels^{2,13} delivered accurate information about the cold scattering properties of Yb, most notably the s -wave scattering lengths for all isotopic combinations. Additionally, intercombination line PAS has provided insight into such exotic physical phenomena as subradiant 1_g states¹⁴ and hyperfine-induced purely-long-range states¹⁵. PA lines near the intercombination line also gives experimentalists the capacity to alter the scattering properties of ultracold Yb atoms optically through the optical Feshbach resonance mechanism^{12,16–18}.

Other excited states of Yb_2 have also been probed in ultracold atom experiments. The s -wave scattering length in the $^1S_0 + ^3P_0$ (0_u^-) state in $^{174}Yb_2$ has been determined through clock spectroscopy of Bose–Einstein condensates trapped in 3D optical lattices^{19,20}. Based on these measurements the positions of near-threshold molecular clock states could be de-

terminated²¹. Orbital Feshbach resonances have been utilized to produce strong correlations²² in a degenerate Fermi gas of ^{173}Yb atoms and create a novel type of Feshbach molecules²³. Collisions of atoms in the ground and metastable $^3\text{P}_2$ states have also been considered: magnetic Feshbach resonances²⁴ and Feshbach molecules²⁵ have been observed experimentally. Feshbach resonances in this pair of states have been shown to exhibit quantum chaos²⁶.

Finally, Yb offers excellent opportunities for tests of fundamental physics. It – uniquely – possesses two independent clock transitions with an unusually high sensitivity to possible variations of the fine structure constant²⁷. Open-shell molecules involving Yb, like RbYb or LiYb can be used in searches for the electric dipole moment of the electron (eEDM)²⁸. Thanks to its simple structure, the ground state Yb dimer is an excellent testing ground for the search for new short scale gravitylike forces²⁹, temporal variations of the proton-to-electron mass ratio³⁰, or beyond-Born-Oppenheimer effects¹³. An “optical molecular clock”²¹ utilizing forbidden $J = 0 \leftrightarrow 0$ transitions between the ground $(1)0_g^+$ and clock $(1)0_u^-$ states in Yb_2 could provide energy level measurements at an accuracy so far unprecedented in molecular spectroscopy.

Despite these advancements, our knowledge of the ground and excited state electronic structures of the Yb_2 dimer and the resulting interaction potentials remain scarce. The detailed knowledge of molecular potential energy curves would be the first step towards the production of deeply bound ultracold molecules via stimulated Raman adiabatic passage (StiRAP)³¹. Unfortunately, the reliable quantum chemical modeling of the Yb_2 dimer is not straightforward and poses a remarkable challenge for present-day quantum chemistry to provide accurate interaction potentials for both the ground and excited states. The large number of correlated electrons combined with a sizable all-electron basis set makes the theoretical modeling of Yb_2 computationally very demanding. Moreover, the Yb atom ($Z=70$) falls into the class of heavy elements and thus requires a relativistic description of the electronic motion. While for a qualitative study it is sufficient to account for scalar relativistic effects only, spin-orbit coupling has to be included in calculations for a quantitative analysis as well as for electron excitation energies. The rather complex interplay between electron correlation and relativistic effects³² impedes routine quantum chemical calculations on the Yb_2 dimer.

To date, the spin-free coupled cluster ground state interaction potential was investigated by Buchachenko *et al.*³³, while reliable van der Waals C_6 coefficients for ground and selected excited states were calculated by Safronova *et al.*³⁴ and Porsev *et al.*³⁵, respectively. The very first attempt to understand and model the low-lying part of the electronic spectrum of Yb_2 has been already performed in 1998 by Wang and Dolg³⁶. In their multi-reference configuration interaction study, they considered potential energy curves resulting from electron excitations from the occupied σ_u and σ_g to the virtual π_u , π_g , σ_g , and σ_u molecular orbitals. Taking into account recent advances in method development for ground and excited states, higher-quality basis sets, and the increase in computation power, it is now possible to deepen our knowledge on the ground and electronic excited states of Yb_2 and provide more reliable benchmark data for potential energy curves (both ground and excited states) that can be exploited in future experimental manipulations of Yb_2 . The main goal of our work is, thus, to provide a reliable description of the ground and electronic excited states potential energy surfaces of the Yb_2 dimer using modern wave function-based quantum chemistry methods.

METHODOLOGY

Basis sets and scalar relativity

In all our calculations, we used the all-electron atomic natural orbital relativistic correlation consistent (ANO-RCC) basis sets available in the OpenMolcas program package, optimized specifically for the 2-nd order Douglas–Kroll–Hess (DKH) Hamiltonian³⁷. We employed the triple- ζ (TZ), quadruple- ζ (QZ), and “large” quality basis sets with the following contraction schemes: $25s22p15d11f4g2h \rightarrow 8s7p4d3f2g$, $25s22p15d11f4g2h \rightarrow 9s8p5d4f3g$, $25s22p15d11f4g2h \rightarrow 11s10p8d7f4g$, respectively. The most accurate calculations for the ground state included a fully uncontracted ANO-RCC basis set and the 5-th order DKH Hamiltonian. We should note that the quality of the calculated potential energy surfaces is not affected by the order of the DKH transformation. Thus, for all other electronic structure methods, scalar relativistic effects were accounted for by the second order Douglas–Kroll–Hess Hamiltonian (DKH2)^{38,39}.

pCCD-based methods

All pair Coupled Cluster Doubles (pCCD)^{40,41} calculations, also known as the Antisymmetric Product of 1-reference orbital Geminal (AP1roG), were performed using our locally developed PIERNIK⁴² software package. The pCCD ansatz can be written as

$$|\text{pCCD}\rangle = \exp\left(\sum_{i=1}^{\text{occ}} \sum_{a=1}^{\text{virt}} t_i^a a_a^\dagger a_{\bar{a}}^\dagger a_{\bar{i}} a_i\right) |0\rangle = e^{\hat{T}_p} |0\rangle, \quad (1)$$

where a_p^\dagger and a_p ($a_{\bar{p}}^\dagger$ and $a_{\bar{p}}$) are the electron creation and annihilation operators for α (β) electrons and $|0\rangle$ is some independent-particle wave function (for instance, the Hartree–Fock (HF) determinant). In eq. (1), $\{t_i^a\}$ are the electron-pair amplitudes and $\hat{T}_p = \sum_{i=1}^{\text{occ}} \sum_{a=1}^{\text{virt}} t_i^a a_a^\dagger a_{\bar{a}}^\dagger a_{\bar{i}} a_i$ is the electron-pair excitation operator that excites an electron pair from an occupied orbital ($i\bar{i}$) to a virtual orbital ($a\bar{a}$) with respect to $|0\rangle$. In all pCCD and post-pCCD calculations, we used different sets of orbitals: canonical Hartree–Fock orbitals and variationally optimized pCCD orbitals (denoted as voo-pCCD)^{43–45}. Furthermore, voo-pCCD calculations were constraint to the D_{2h} and C_{2v} point group symmetry, respectively. The missing dynamical energy correction on top of pCCD/voo-pCCD was included via a linearized coupled cluster correction⁴⁶, denoted as pCCD-LCCSD.

Moreover, three variants of the equation of motion (EOM) coupled cluster model to target excited states within the pCCD formalism were investigated. First, the EOM formalism was directly applied on top of the pCCD reference. Single excitations were included *a posteriori* in the EOM ansatz, that is, the linear excitation operator of the EOM formalism is limited to pair and single excitations. This approach is denoted as EOM-pCCD+S^{47,48}. The second model includes single excitations also in the coupled cluster reference function. These single excitations are included on top of the pCCD reference function. This method is labeled as pCCD-CCS, while the excited state extension is abbreviated as EOM-pCCD-CCS. Finally, in the most accurate EOM variant, the pCCD reference was replaced by the pCCD-LCCSD function, resulting in the EOM-pCCD-LCCSD approach^{49,50}.

EOM-CCSD/CCSD(T)

All CCSD(T)⁵¹ and EOM-CCSD⁵² calculations were carried out in the MOLPRO2012 software package^{53–56} using D_{2h} point group symmetry.

CASSCF/SO-CASPT2

The Complete Active Space Self Consistent Field (CASSCF)^{57,58} calculations and Complete Active Space Second-order Perturbation Theory (CASPT2)^{59–61} calculations were performed in the D_{2h} point group symmetry using the OpenMolcas (version 17.0) software package^{62–65}. The CASSCF wave functions were used to calculate multistate CASPT2 energy corrections, where the ionization potential-electron affinity (IPEA) shifted H_0 Hamiltonian⁶⁶ was applied with an imaginary shift set to 0.25. The spin-orbit (SO) interaction effects (in the Atomic Mean Field Approximation^{67–69}) were calculated using the Restricted Active Space State Interaction (RASSI) approach,⁷⁰ where the energy correction due to dynamical correlation was included in an approximate manner by dressing the diagonal elements of the spin-orbit Hamiltonian by the CASPT2 energies. Throughout this work, we utilized the state averaged CASSCF approach combined with the subsequent RASSI/SO calculations with the same active space sizes as in CASSCF. In the Yb atomic calculations, we employed two active space variants: CAS(2,4)SCF with the 6s and 6p orbitals correlated and CAS(2,9)SCF augmented by the additional 5d orbitals. For the Yb₂ molecule, we performed CAS(4,8)SCF calculations which comprised occupied σ_u (Yb 6s) and σ_g (Yb 6s) orbitals as well as virtual σ_g (Yb 6p_z), σ_u (Yb 6p_z), π_u (Yb 6p_x/p_y), and π_g (Yb 6p_x/p_y) molecular orbitals.

Fitting procedure

All potential energy curves were obtained from a polynomial fit of 8-th order. The corresponding spectroscopic constants (equilibrium bond length (r_e) and harmonic vibrational frequency (ω_e)) were calculated based on those fitted potential energy curves. Specifically, the harmonic vibrational frequencies (ω_e) were determined numerically using the five-point finite difference stencil⁷¹ and the average mass of ytterbium, that is, 173.045.⁷² The potential energy depth (D_e) was evaluated as the difference between the atomic limit and the

minimum energy of a given potential energy curve. Note that in pCCD-based calculations employing D_{2h} point group symmetry the dissociation energies were estimated by adding the corresponding atomic excitation energies to the dissociation limit of the dimer calculation. This step had to be performed due to size-consistency problems in the pCCD reference function. If the orbitals are allowed to relax freely, the size-consistency error is eliminated and the dissociation limits of the dimer calculation numerically agree with the atomic ground and excited state energies.

RESULTS and DISCUSSION

The electronic structure of the ytterbium atom

Ytterbium is a closed-shell atom described by the ground-state 1S_0 term. Its valence electronic configuration is characterized by the fully occupied 4f and 6s subshells and the low-lying unoccupied 5p, 5d, and 7s subshells. Despite its closed-shell electronic nature, the ytterbium atom has a rather complex electronic structure, which manifests itself in close-lying potential energy levels^{72,73}. Specifically, in the range of 17 000 to 50 000 cm^{-1} , there is a large number of quasi-degenerate states that are characterized by electron transfer not only from the occupied 6s to the unoccupied 5p, 5d, 7s, and 8s orbitals, but also from the occupied 4f (7-fold) semi-core orbitals. This peculiar electronic structure leads to a large number of low-lying excited states and a very dense electronic spectrum, for some of which atomic term symbols are difficult to assign^{72,73}.

In this work, we focus on the low-lying energy levels of the Yb atom arising from the occupied 6s to the unoccupied 5p and 5d orbitals. Specifically, we use the experimentally determined energy levels available in Refs. 72,73 as a starting point to assess the accuracy of different quantum chemistry methods. Since not all quantum chemistry methods used in this work are directly applicable to triplet excited states (EOM-based approaches), we first focus on the lowest-lying 1D ($6s \rightarrow 5d$) and 1P ($6s \rightarrow 6p$) energy levels of Yb. The corresponding results are summarized in Table 1.

All excited state methods correctly place the 1P state below 1D ; nonetheless, the splitting

Main config.	Term	Spin-free levels [cm^{-1}]						
		EOM				CAS(2,9)		Exp.*
		pCCD+S	pCCD-CCS	pCCD-LCCSD	CCSD	CASSCF	CASPT2	Ref. 72
4f ¹⁴ 6s6p	¹ P	29 131	29 127	26 452	25 826	24 672	25 007	24 964
4f ¹⁴ 6s5d	¹ D	29 414	29 355	29 303	30 182	27 840	27 574	27 628

* The empirical positions 24 964 cm^{-1} and 18 903 cm^{-1} respectively of spin-free ¹P and ³P states were determined from experimental positions of ¹P₁ and ³P_{0,1,2} states using the spin-orbit Hamiltonian in Ref. 74 and take into account the mutual repulsion between ³P₁ and ¹P₁ states. Analogously, the empirical positions of spin-free ¹D and ³D states are 27 628 cm^{-1} and 24 958 cm^{-1} , respectively, and account for the repulsion between the ¹D₂ and ³D₂ states.

Table 1: Singlet electronic energy levels of the Yb atom calculated from different quantum chemistry methods using the TZ-ANO-RCC basis set (in cm^{-1}). The energy of the ¹S ground state (electronic configuration 4f¹⁴6s²) equals zero for all theoretical models and experiment.

between these two states differs for all investigated approaches. All considered EOM-based theories overestimate the energy of the ¹D level by approximately 2 000 cm^{-1} . The ¹P state is rather accurately predicted by the standard EOM-CCSD method, followed by EOM-pCCD-LCCSD. For more simplified EOM models, however, larger deviations from the reference value are observed (differences amount to 3 000 cm^{-1}). This results in underestimated energy splittings between the ¹P and ¹D terms. On the other hand, spin-free CASSCF and CASPT2 electronic spectra match very well the experimental energy levels mentioned in Table 1. The overall deviations do not exceed 300 and 100 cm^{-1} for CASSCF and CASPT2, respectively.

The Yb energy levels obtained from SO-CAS(2,4)PT2 and SO-CAS(2,9)PT2 combined with various basis set sizes are presented in Tables 2 and 3. Both active spaces qualitatively reproduce the experimental energy levels of the Yb atom with respect to the energetic order and magnitude of spin-orbit splittings. The largest differences between the CAS(2,4) and CAS(2,9) variants are observed for the ¹P state, which is underestimated by about 2 000 cm^{-1} in the smaller CAS. This shift in energy highlights the importance of unoccupied d-type orbitals in post-Hartree-Fock calculations, similar to the *double d-shell effect* in 3d transition

metal chemistry.⁷⁵ In both active space calculations, dynamic energy corrections seem to be important and amount to 500–2 000 cm⁻¹ for a given energy level. Finally, we should note that the quality of excitation energies in the Yb atom seems to be rather insensitive to the basis set quality. Only minor changes in the order of states are observed and amount to a few hundreds of cm⁻¹ (cf. Table 3). These observations point to a well-balanced, good quality ANO-RCC basis set for valence atomic properties of the Yb atom.

Basis	Main config.	Term	Spin-free levels [cm ⁻¹]			Spin-orbit levels [cm ⁻¹]		
			CAS(2,4)SCF	CASPT2	Exp.* 72	J	SO-CASPT2	Exp. 72
TZ-ANO-RCC	4f ¹⁴ 6s6p	³ P	16 304	17 123	18 903	0	15 965	17 288
						1	16 523	17 992
						2	17 704	19 710
	4f ¹⁴ 46s6p	¹ P	29 608	28 011	24 964	1	28 041	25 068
QZ-ANO-RCC	4f ¹⁴ 6s6p	³ P	16 315	17 207	18 903	0	16 074	17 288
						1	16 628	17 992
						2	17 779	19 710
	4f ¹⁴ 46s6p	¹ P	28 966	27 430	24 964	1	27 453	25 068
large-ANO-RCC	4f ¹⁴ 6s6p	³ P	16 315	17 256	18 903	0	16 120	17 288
						1	16 675	17 992
						2	17 828	19 710
	4f ¹⁴ 6s6p	¹ P	28 512	27 025	24 964	1	27 046	25 068

* See the footnote below Table 1.

Table 2: Electronic energy levels of the Yb atom calculated from the SO-CAS(2,4)PT2 approach and different quality ANO-RCC basis sets (in cm⁻¹). The energy of the ¹S ground state (electronic configuration 4f¹⁴6s²) equals zero for all theoretical models and experiment.

Towards a reliable and accurate ground state potential energy surface for the Yb₂ dimer

When the two Yb atoms approach each other, they create a weakly-bonded, van der Waals-type complex.^{33,36,76,77} It is well-known that such weakly-bonded compounds tend to be extremely sensitive to the quality of the atomic basis set and the (approximate) dynamic en-

Basis	Main config.	Term	Spin-free levels [cm ⁻¹]			Spin-orbit levels [cm ⁻¹]		
			CAS(2,4)SCF	CASPT2	Exp.* 72	J	SO-CASPT2	Exp. 72
TZ-ANO-RCC	4f ¹⁴ 6s6p	³ P	15 497	16 694	18 903	0	15 528	17 288
						1	16 064	17 992
						2	17 276	19 710
	4f ¹⁴ 6s5d	³ D	26 895	25 684	24 958	1	25 149	24 489
						2	25 443	24 752
						3	26 040	25 271
	4f ¹⁴ 46s6p	¹ P	24 672	25 007	24 964	1	25 053	25 068
	4f ¹⁴ 46s5d	¹ D	27 840	27 574	27 628	2	27 690	27 678
QZ-ANO-RCC	4f ¹⁴ 6s6p	³ P	15 416	16 862	18 903	0	15 720	17 288
						1	16 249	17 992
						2	17 433	19 710
	4f ¹⁴ 6s5d	³ D	26 573	25 124	24 958	1	24 614	24 489
						2	24 899	24 752
						3	25 474	25 271
	4f ¹⁴ 46s6p	¹ P	24 275	24 793	24 964	1	24 834	25 068
	4f ¹⁴ 46s5d	¹ D	27 485	27 142	27 628	2	27 265	27 678
large-ANO-RCC	4f ¹⁴ 6s6p	³ P	15 381	16 997	18 903	0	15 870	17 288
						1	16 399	17 992
						2	17 560	19 710
	4f ¹⁴ 6s5d	³ D	26 414	24 423	24 958	1	23 909	24 489
						2	24 202	24 752
						3	24 747	25 271
	4f ¹⁴ 6s6p	¹ P	24 170	24 848	24 964	1	24 888	25 068
	4f ¹⁴ 6s5d	¹ D	27 191	26 373	27 628	2	26 500	27 678

* See the footnote below Table 1.

Table 3: Electronic energy levels of the Yb atom calculated from the SO-CAS(2,9)PT2 approach and different quality ANO-RCC basis sets (in cm⁻¹). The energy of the ¹S ground state (electronic configuration 4f¹⁴6s²) equals zero for all theoretical models and experiment.

ergy correction.⁷⁸ Thus, we first scrutinize the ground state potential energy surface obtained from the CCSD(T) approach before benchmarking various electron correlation methods for both ground and excited states.

Reference ground-state potential energy curve

Table 4 summarizes the influence of the number of correlated electrons on the quality of the CCSD and CCSD(T) potential energy surfaces, respectively, including their spectroscopic constants (optimal bond lengths (r_e), harmonic vibrational frequencies (ω_e), and potential energy depths (D_e)). To minimize the basis set superposition error⁷⁹ we employed the all-

electron uncontracted ANO-RCC basis set. Our calculations suggest that it is necessary to correlate all occupied orbitals starting from the fourth atomic shell of the Yb atom (see Table 4), that is, 84 electrons of the Yb dimer have to be correlated in a calculation. Correlating additional core electrons does not considerably change the spectroscopic constants of Yb₂. Our most accurate CCSD(T) prediction yields an optimal bond length of $r_e = 8.814$ bohr, a harmonic vibrational frequencies of $\omega_e = 21 \text{ cm}^{-1}$, and a potential energy depth of $D_e = 579 \text{ cm}^{-1}$. The computed harmonic vibrational frequency matches the experimental value of 22 cm^{-1} measured by Goodfriend⁸⁰. It is important to note that restricting the number of correlated electrons to 32 or less shifts the optimal bond length towards longer inter-atomic distances and overestimates the potential energy depth. Neglecting contributions from triply-excited determinants (as in CCSD) elongates the optimal bond length by approximately 0.4 bohr and lowers the vibrational frequencies and potential energy depth. The latter is most significantly affected by the lack of triple excitations in the cluster operator, where the differences in D_e between CCSD and CCSD(T) amount to $250\text{--}300 \text{ cm}^{-1}$ (a difference of approximately 40%, see also Table 4). Analysis of the t_1 diagnostic⁸¹ in CCSD along potential energy surface shows a single-reference nature of the Yb₂ ground-state (values in the order of 0.02). Finally, we should mention that our new best estimate for the potential energy depth, $D_e = 579 \text{ cm}^{-1}$, is lower than the recently reported value of $D_e = 786 \text{ cm}^{-1}$ by Mosyagin and coworkers⁸², who employed a smaller basis set and different approaches to electron correlation and relativistic effects.

Assessing the accuracy of conventional and unconventional quantum chemistry approaches in modeling the ground state potential energy surface

The CCSD potential energy curve can be used as a reference to evaluate the reliability of simplified coupled cluster methods that include at most double excitations. Table 5 lists the spectroscopic constants obtained from various quantum chemistry methods and a given basis set. Including an LCCSD dynamic energy correction on top of the pCCD reference wavefunction is indispensable for obtaining qualitatively correct bond lengths. Furthermore, the potential energy depth heavily depends on the type of orbitals used in the pCCD reference calculations (canonical Hartree–Fock or variationally optimized orbitals imposing C_{2v} and

method	correlated occupied orbitals	N_e	$r_e[\text{a}_0]$	$\omega_e[\text{cm}^{-1}]$	$D_e[\text{cm}^{-1}]$
CCSD	6s	4	9.438	17	365
CCSD	5s, 5p, 6s	20	9.373	16	342
CCSD	4f, 6s	32	9.293	16	345
CCSD	5p, 4f, 6s	44	9.281	16	328
CCSD	5s, 5p, 4f, 6s	48	9.277	16	336
CCSD	4s, 4p, 4d, 5s, 5p, 4f, 6s	84	9.260	16	336
CCSD	3s, 3p, 3d, 4s, 4p, 4d, 5s, 5p, 4f, 6s	120	9.266	16	336
CCSD	1s, 2s, 2p, 3s, 3p, 3d, 4s, 4p, 4d, 5s, 5p, 4f, 6s	140	9.265	16	336
CCSD(T)	6s	4	9.050	22	645
CCSD(T)	5s, 5p, 6s	20	8.968	21	592
CCSD(T)	4f, 6s	32	8.874	21	591
CCSD(T)	5p, 4f, 6s	44	8.822	21	579
CCSD(T)	5s, 5p, 4f, 6s	48	8.810	21	585
CCSD(T)	4s, 4p, 4d, 5s, 5p, 4f, 6s	84	8.815	21	580
CCSD(T)	3s, 3p, 3d, 4s, 4p, 4d, 5s, 5p, 4f, 6s	120	8.814	21	579
CCSD(T)	1s, 2s, 2p, 3s, 3p, 3d, 4s, 4p, 4d, 5s, 5p, 4f, 6s	140	8.814	21	579

Table 4: CCSD and CCSD(T) spectroscopic constants for the Yb_2 $X^1\Sigma_g^+$ state using uncontracted ANO-RCC basis set and a varying number of active (occupied) orbitals and thus correlated electrons. N_{corr} denotes the number of correlated electrons, r_e the equilibrium bond length, ω_e the vibrational frequency, and D_e the potential depth, respectively. The occupied orbitals not included in the set of correlated orbitals (second column) were kept frozen during CCSD(T) calculations. All virtual orbitals were correlated.

D_{2h} point group symmetry). The best agreement of all pCCD-based methods with CCSD (as well as with CCSD(T) reference) data is obtained when the point group symmetry is lowered and the orbitals are thus allowed to (partially) localize in the dimer calculation. Note that orbital optimization in pCCD typically involves localization.^{83,84} CAS(4,8)PT2 results in overly bond lengths and underestimated low vibrational frequencies compared to CCSD calculations (employing the same basis set). Increasing the basis set size in CAS(4,8)PT2 improves the agreement between CCSD and CASPT2 data. The slower convergence of the second-order perturbation theory approach with basis set size for weakly interacting systems is not surprising and has been reported earlier in the literature⁸⁵. As to be expected, inclusion of spin-orbit coupling does not significantly affect the quality of the CAS(4,8)PT2 ground-state potential energy curve. To this end, we can conclude that both the pCCD-LCCSD(C_{2v})

and CAS(4,8)PT2 methods are promising alternatives for modeling excited state potential energy curves in the Yb₂ dimer.

method	N _e	basis	r _e [a ₀]	ω _e [cm ⁻¹]	D _e [cm ⁻¹]
CCSD	48	TZ-ANO-RCC	8.684	24	956
pCCD	48	TZ-ANO-RCC	10.004	14	361
pCCD(<i>D</i> _{2h})	48	TZ-ANO-RCC	8.604	27	1 046
pCCD(<i>C</i> _{2v})	48	TZ-ANO-RCC	13.674	22	22
pCCD-LCCSD	48	TZ-ANO-RCC	8.102	36	1 875
pCCD-LCCSD(<i>D</i> _{2h})	48	TZ-ANO-RCC	7.852	42	2 609
pCCD-LCCSD(<i>C</i> _{2v})	48	TZ-ANO-RCC	8.467	26	785
CAS(4,8)PT2	4/32	TZ-ANO-RCC	11.381	13	280
CAS(4,8)PT2	4/32	QZ-ANO-RCC	10.998	11	256
CAS(4,8)PT2	4/32	large-ANO-RCC	8.837	19	369
SO-CAS(4,8)PT2	4/32	TZ-ANO-RCC	10.751	11	221
SO-CAS(4,8)PT2	4/32	QZ-ANO-RCC	10.463	9	259
SO-CAS(4,8)PT2	4/32	large-ANO-RCC	8.519	24	409

Table 5: Spectroscopic constants for the Yb₂ X ¹Σ_g⁺ state from different quantum chemistry methods. N_{corr} denotes the number of correlated electrons, r_e equilibrium bond length, ω_e vibrational frequency, and D_e potential depth, respectively.

Yb₂ excited-state properties

Examination of the electronic structure of the Yb atom points to the importance of the 4*f*, 6*s*, 6*p*, and 5*d* atomic orbitals in the electronic spectrum of Yb₂. Including all these orbitals in active space calculations is prohibitive and some compromise has to be made. A reasonable choice would be to correlate only the 6*s*, 6*p*, and 5*d* atomic orbitals in molecular Yb₂ calculations, that is, performing CAS(4,18)SCF calculations. Unfortunately, such an active space is not stable along the potential energy surface, where smooth potential energy curves for all excited states of interest cannot be optimized due to technical difficulties. As a consequence, we had to reduce the number of active orbitals and neglected the contributions from 5*d* orbitals by moving them outside the CAS space (into the external space). This results in our CAS(4,8)SCF model that is further used as reference for all Yb₂ excited states

potential energy curves. We should stress that the same active space was used in previous ECP/MRCI calculations³⁶.

Reference spin-free electronic spectrum

Table 6 collects all spin-free spectroscopic constants obtained from CAS(4,8)PT2 using different sizes for the atomic basis set. Similar to the ground state calculations, the CAS(4,8)PT2 spectroscopic constants converge very slowly with basis set size. In general, incrementing the basis set size shortens bond lengths, marginally increases vibrational frequencies, deepens potential energy depths, and lowers the adiabatic excitation energies. The CAS(4,8)PT2 results obtained using the TZ-ANO-RCC basis set qualitatively match the ECP/MRCI³⁶ spectroscopic constants (cf. Table 6). The largest discrepancies are observed for the higher-lying $^1\Pi_u$ and $^1\Sigma_g^+$ excited states, where the differences in excitation energies amount to few thousand wave numbers. The agreement between ECP/MRCI and all-electron CAS(4,8)PT2 spectroscopic parameters decreases for larger basis sets, indicating the need for decent basis set sizes to reliably describe excited-state potential energy surfaces of Yb_2 . The discrepancies between ECP/MRCI and CAS(4,8)PT2 can be attributed to the different treatment of scalar relativistic and electron correlation effects in both approaches. One should keep in mind that any truncated CI approach, such as MRCI, is not rigorously size-extensive and size-consistent, while CASPT2 is, in general, size-extensive and approximately size-consistent. Thus, we believe that our CAS(4,8)PT2 results can be considered as new reference data for the excited potential energy curves of the Yb_2 dimer. We further hope that future experiments on laser induced fluorescence will help to resolve this ambiguity.

Singlet excitation energies from EOM-based methods

Having generated reference excited-state potential energy curves, we can now assess the accuracy of (simplified) EOM-based methods for singlet excitation energies. Table 7 lists all the spectroscopic constants for excited states obtained from various flavours of EOM methods and their difference with respect to the CAS(4,8)PT2 data. In general, the EOM-based excited state energies are overestimated and the potential energy depths underestimated compared to CAS(4,8)PT2 results. These differences are smaller when an LCCSD correction is applied on top of pCCD, pushing the EOM-pCCD-LCCSD results very close to

State	basis	r_e [a_0]	ω_e [cm^{-1}]	D_e [cm^{-1}]	T_e [cm^{-1}]	Dissociation limit
$^3\Pi_g$	TZ-ANO-RCC	6.955	69	6 255	11 147	$^1S + ^3P$
	QZ-ANO-RCC	6.890	69	6 640	10 823	$^1S + ^3P$
	large-ANO-RCC	6.794	73	7 566	10 059	$^1S + ^3P$
	ECP(MRCI) ³⁶	6.680	77	8 065	12 421	$^1S + ^3P$
$^1\Pi_g$	TZ-ANO-RCC	6.751	79	15 776	12 514	$^1S + ^1P$
	QZ-ANO-RCC	6.688	77	15 684	12 002	$^1S + ^1P$
	large-ANO-RCC	6.612	80	16 364	11 030	$^1S + ^1P$
	ECP(MRCI) ³⁶	6.546	84	14 841	13 389	$^1S + ^1P$
$^3\Sigma_u^+$	TZ-ANO-RCC	7.697	56	4 141	13 261	$^1S + ^3P$
	QZ-ANO-RCC	7.636	57	4 493	12 970	$^1S + ^3P$
	large-ANO-RCC	7.578	61	5 315	12 310	$^1S + ^3P$
	ECP(MRCI) ³⁶	7.559	58	5 162	15 325	$^1S + ^3P$
$^3\Pi_u$	TZ-ANO-RCC	8.835	21	425	16 978	$^1S + ^3P$
	QZ-ANO-RCC	8.693	22	522	16 942	$^1S + ^3P$
	large-ANO-RCC	8.374	31	802	16 824	$^1S + ^3P$
	ECP(MRCI) ³⁶	8.343	24	1 048	19 438	$^1S + ^3P$
$^1\Sigma_u^+$	TZ-ANO-RCC	7.513	48	8 774	19 516	$^1S + ^1P$
	QZ-ANO-RCC	7.307	52	8 906	18 781	$^1S + ^1P$
	large-ANO-RCC	7.078	60	10 405	16 989	$^1S + ^1P$
	ECP(MRCI) ³⁶	7.359	53	7 824	20 406	$^1S + ^1P$
$^1\Pi_u$	TZ-ANO-RCC	7.258	71	5 595	22 695	$^1S + ^1P$
	QZ-ANO-RCC	7.273	67	5 455	22 232	$^1S + ^1P$
	large-ANO-RCC	7.223	69	6 124	21 270	$^1S + ^1P$
	ECP(MRCI) ³⁶	7.319	56	1 936	26 294	$^1S + ^1P$
$^1\Sigma_g^+$	TZ-ANO-RCC	7.664	68	5 111	23 179	$^1S + ^1P$
	QZ-ANO-RCC	7.461	71	5 008	22 679	$^1S + ^1P$
	large-ANO-RCC	7.856	49	4 727	22 667	$^1S + ^1P$
	ECP(MRCI) ³⁶	7.529	58	1 613	26 616	$^1S + ^1P$

Table 6: Adiabatic spin-free electronic spectrum of Yb_2 from CAS(4,8)PT2 using different ANO-RCC basis sets. r_e denotes the equilibrium bond length, ω_e vibrational frequency, D_e potential depth, and T_e adiabatic excitation energy, respectively. The $^3\Sigma_g^+$ state does not have a minimum and thus its spectroscopic constants are not calculated.

EOM-CCSD data. Opposite to what we observed for the ground-state, the best performance of EOM-pCCD-LCCSD is achieved when D_{2h} point group symmetry is imposed. The largest discrepancies between EOM-pCCD-LCCSD and EOM-CCSD can be found for the $^1\Sigma_g^+$ excited state. Specifically, this excited state features a strong multi-reference nature with a

double electron excitation character. It is well known that such bi-excited states cannot be correctly described by the standard (single-reference) EOM-CCSD framework. Recent work on all-trans polyene chains highlights the superiority of EOM-pCCD-based methods to correctly describe double electron excitation energies^{47–49}. The same is true for the ${}^1\Sigma_g^+$ excited state in the Yb₂ dimer. Thus, pCCD-based excited state methods outperform the conventional EOM-CCSD formalism. Figure 1 shows the evolution of the bi-excitation character in the ${}^1\Sigma_g^+$ excited state along the potential energy surface. For short inter-atomic distances the doubly-excited state has a dominant contribution in all investigated methods, except for EOM-CCSD. Moreover, all EOM-pCCD-type approaches feature a similar evolution of the contribution of doubly-excited states along the ${}^1\Sigma_g^+$ Yb₂ potential energy surface, which qualitatively agrees with CAS(4,8)SCF results. We should note that the excitation contributions to the ${}^1\Sigma_g^+$ excited state in EOM-pCCD-LCCSD(C_{2v}) are reversed in contrast to all remaining pCCD-based methods. The orbital optimization and (partial) orbital localization thus lowers the bi-excited character in the ${}^1\Sigma_g^+$ state. While this observed symmetry-breaking worsens equilibrium bond lengths and vibrational frequencies, excitation energies deviate less compared to the CAS(4,8)PT2 reference values. Finally, we should stress that EOM-pCCD-LCCSD(D_{2h}) in general outperforms EOM-CCSD in predicting spectroscopic constants for the lowest-lying excited states (difference amount to 2 500 cm⁻¹).

Reference spin-orbit electronic spectrum

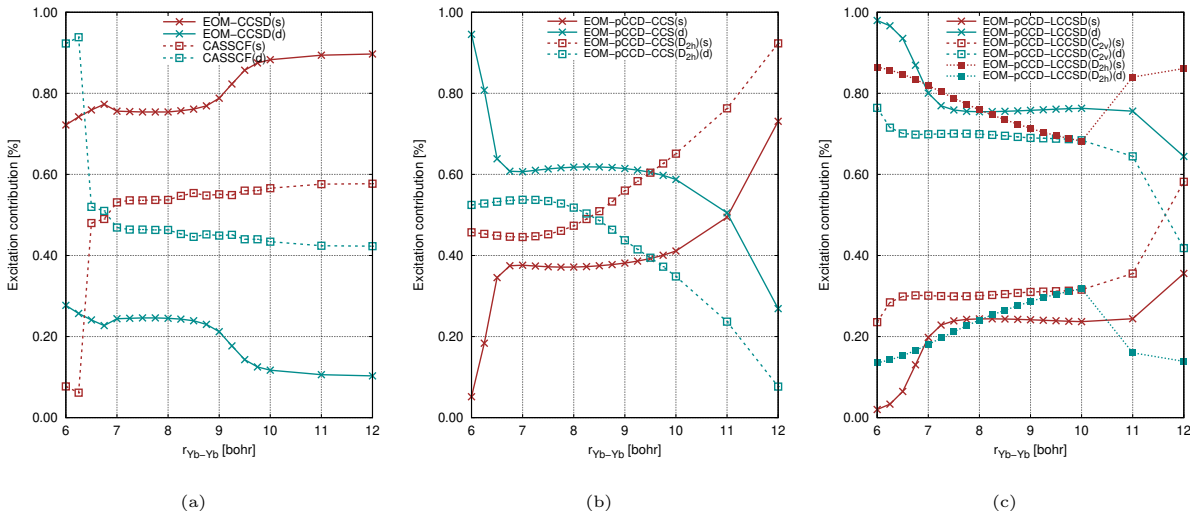
The reference spin-orbit Yb₂ excited-state potential energy surfaces are presented in Figure 2. If spin-orbit coupling is accounted for, the minima of each excited potential energy curve are shifted towards shorter inter-atomic distances. Furthermore, the whole spectrum is rather dense, especially all states approaching the atomic limits ${}^1S+{}^3P_0$, ${}^1S+{}^3P_1$, and ${}^1S+{}^3P_2$ lie very close to each other. Higher lying are the $1_u({}^1\Pi_u)$ and $0_g^+({}^1\Sigma_g^+)$ states that dissociate into the ${}^1S+{}^1P_1$ atomic limit. A distinct feature of the Yb₂ electronic spectrum is the presence of 0_g^+ excited states originating from the repulsive (spin-free) ${}^3\Sigma_g^+$ state with a specific shape of the potential energy surface compared to the remaining excited states.

The SO-CAS(4,8)PT2 spectroscopic parameters for the excited states in Yb₂ are collected in Tables 8–11. For convenience, the spectroscopic characteristics of all investigated excited

State	Method	r_e [a ₀]	ω_e [cm ⁻¹]	D_e [cm ⁻¹]	T_e [cm ⁻¹]
¹ Π _g	EOM-CCSD	6.643 (-0.031)	81 (1)	13 773 (-2 591)	13 035 (2 005)
	EOM-pCCD+S	7.100 (0.488)	71 (-9)	13 596 (-2 768)	15 904 (4 874)
	EOM-pCCD+S(<i>D</i> _{2h})	6.993 (0.381)	72 (-8)	14 347 (-2 017)	15 829 (4 799)
	EOM-pCCD-CCS	7.091 (0.479)	71 (-9)	13 712 (-2 652)	15 775 (4 745)
	EOM-pCCD-CCS(<i>D</i> _{2h})	6.992 (0.380)	72 (-8)	14 350 (-2 014)	15 837 (4 807)
	EOM-pCCD-LCCSD	6.562 (-0.050)	82 (2)	15 047 (-1 317)	13 276 (2 246)
	EOM-pCCD-LCCSD(<i>D</i> _{2h})	6.561 (-0.051)	84 (4)	16 046 (-318)	13 134 (2 104)
	EOM-pCCD-LCCSD(<i>C</i> _{2v})	6.588 (-0.024)	82 (2)	14 696 (-1 668)	13 862 (2 832)
¹ Σ _u ⁺	EOM-CCSD	7.693 (0.615)	47 (-13)	6 788 (-3Åa617)	19 996 (3Åa007)
	EOM-pCCD+S	8.889 (1.811)	31 (-29)	7 163 (-3Åa242)	22 337 (5Åa348)
	EOM-pCCD+S(<i>D</i> _{2h})	8.823 (1.745)	33 (-27)	6 831 (-3Åa574)	23 345 (6Åa356)
	EOM-pCCD-CCS	8.931 (1.853)	31 (-29)	7 095 (-3 319)	22 392 (5 403)
	EOM-pCCD-CCS(<i>D</i> _{2h})	8.821 (1.743)	33 (-27)	6 851 (-3 554)	23 337 (6 348)
	EOM-pCCD-LCCSD	7.575 (0.497)	48 (-12)	7 682 (-2Åa723)	20 641 (3 652)
	EOM-pCCD-LCCSD(<i>D</i> _{2h})	7.448 (0.370)	51 (-9)	8 647 (-1 758)	20 532 (3 543)
	EOM-pCCD-LCCSD(<i>C</i> _{2v})	7.441 (0.363)	49 (-11)	8 075 (-2 330)	20 484 (3 495)
¹ Π _u	EOM-CCSD	7.488 (0.265)	48 (-21)	3 610 (-2 514)	27 529 (6 259)
	EOM-pCCD+S(HF)	8.128 (0.905)	43 (-26)	1 689 (-4 435)	27 811 (6 541)
	EOM-pCCD+S(<i>D</i> _{2h})	7.802 (0.579)	53 (-16)	2 604 (-3 520)	27 572 (6 302)
	EOM-pCCD-CCS	7.995 (0.772)	47 (-22)	1 785 (-4 339)	27 702 (6 432)
	EOM-pCCD-CCS(<i>D</i> _{2h})	7.800 (0.577)	54 (-15)	2 611 (-3 513)	27 577 (6 307)
	EOM-pCCD-LCCSD	7.300 (0.077)	63 (-6)	2 882 (-3 242)	25 310 (4 040)
	EOM-pCCD-LCCSD(<i>D</i> _{2h})	7.226 (0.003)	67 (-2)	3 574 (-2 550)	25 025 (3 755)
	EOM-pCCD-LCCSD(<i>C</i> _{2v})	7.296 (0.073)	62 (-7)	2 039 (-4 085)	25 875 (4 605)
¹ Σ _g ⁺	EOM-CCSD	7.757 (-0.099)	54 (5)	1 232 (-3 495)	26 683 (4 016)
	EOM-pCCD+S	8.083 (0.227)	59 (10)	6 961 (2 234)	22 539 (-128)
	EOM-pCCD+S(<i>D</i> _{2h})	7.621 (-235)	79 (30)	7 229 (2 502)	22 947 (280)
	EOM-pCCD-CCS	8.095 (0.239)	67 (18)	7 056 (2 329)	22 432 (-235)
	EOM-pCCD-CCS(<i>D</i> _{2h})	7.620 (-0.236)	79 (30)	7 236 (2 509)	22 951 (284)
	EOM-pCCD-LCCSD	7.749 (-0.107)	57 (8)	7 607 (2 880)	20 716 (-1 951)
	EOM-pCCD-LCCSD(<i>D</i> _{2h})	7.507 (-0.349)	70 (21)	8 117 (3 390)	21 063 (-1 604)
	EOM-pCCD-LCCSD(<i>C</i> _{2v})	7.127 (-0.729)	72 (23)	3 661 (-1 066)	24 898 (2 232)

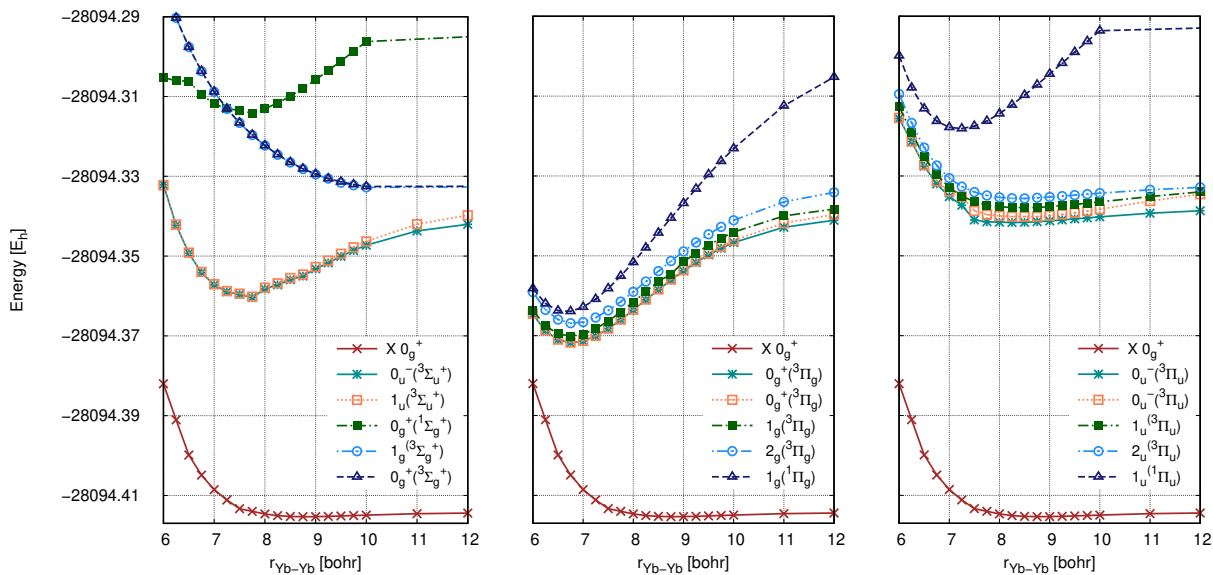
Table 7: Spectroscopic constants for the low-lying adiabatic singlet-excited states of Yb₂ obtained from different EOM-based methods and for the TZ-ANO-RCC basis set. T_e denotes the adiabatic excitation energy, r_e the equilibrium bond length, ω_e the vibrational frequency, and D_e the potential depth, respectively. The labels “(*D*_{2h})” and “(*C*_{2v})” indicate the orbital optimized reference ground state within pCCD, imposing *D*_{2h} and *C*_{2v} point group symmetries, respectively. The differences with respect to the reference CAS(4,8)PT2 values (large-ANO-RCC) are given in parenthesis.

Figure 1: Contributions from single (red) and double (turquoise) excitations in the first $^1\Sigma_g^+$ excited state of Yb_2 from different quantum chemistry methods: (a) EOM-CCSD and CAS(4,8)SCF, (b) EOM-pCCD-CCS (with and without orbital optimization), and (c) EOM-pCCD-LCCSD (with and without orbital optimization and different point group symmetries). Results for EOM-pCCD+S are similar to EOM-pCCD-CCS and are thus not shown in the Figure. For CAS(4,8)SCF, the individual contributions are determined from the weights of all active space configurations with coefficients larger than 0.05 only.



states are grouped into four blocks according to their atomic dissociation limit, Table 8 for the $^1\text{S}+^3\text{P}_0$, Table 9 for the $^1\text{S}+^3\text{P}_1$, Table 10 for the $^1\text{S}+^3\text{P}_2$, and Table 11 for the $^1\text{S}+^1\text{P}_1$ atomic limits, respectively. In the lowest-lying part of the spectrum, our TZ-ANO-RCC results qualitatively match the ECP/SO-MRCI spectroscopic parameters determined by Wang and Dolg³⁶. The differences increase, however, when larger basis sets are used within the SO-CAS(4,8)PT2 approach. This observation suggests the need for large basis set sizes when targeting excited states in the Yb_2 dimer. In general, the size of the atomic basis set affects all spectroscopic parameters. A large basis set considerably shortens the optimal bond lengths, lowers the adiabatic excitation energies, and increases potential energy depths. Harmonic vibrational frequencies are only slightly altered by the choice of the basis set.

Figure 2: SO-CAS(4,8)PT2 electronic spectrum of Yb₂ using the large-ANO-RCC basis set. The whole spectrum is divided into contributions from Σ , Π_u , and Π_g states (from left to right).



State	basis	r_e [a ₀]	ω_e [cm ⁻¹]	D_e [cm ⁻¹]	T_e [cm ⁻¹]
$0_g^-(^3\Pi_g)$	TZ-ANO-RCC	6.938	69	5 627	10 589
	QZ-ANO-RCC	6.874	70	6 038	10 294
	large-ANO-RCC	6.778	73	6 968	9 561
	ECP(MRCI) ³⁶	6.969	65	4 759	13 147
$0_u^-(^3\Sigma_u^+)$	TZ-ANO-RCC	7.693	54	3 132	13 084
	QZ-ANO-RCC	7.640	56	3 506	12 826
	large-ANO-RCC	7.568	60	4 332	12 197
	ECP(MRCI) ³⁶	7.544	54	2 662	15 244

Table 8: SO-CAS(4,8)PT2 adiabatic electronic states of Yb₂ dissociating into the $^1S+^3P_0$ atomic limit. r_e denotes the equilibrium bond length, ω_e the vibrational frequency, D_e the potential depth, and T_e the adiabatic excitation energy, respectively.

State	basis	r_e [a ₀]	ω_e [cm ⁻¹]	D_e [cm ⁻¹]	T_e [cm ⁻¹]
$0_g^+(^3\Pi_g)$	TZ-ANO-RCC	6.939	69	6 173	10 600
	QZ-ANO-RCC	6.877	70	6 584	10 303
	large-ANO-RCC	6.784	73	7 508	9 578
	ECP(MRCI) ³⁶	6.971	66	5 404	13 147
$1_g(^3\Pi_g)$	TZ-ANO-RCC	6.920	69	5 775	10 998
	QZ-ANO-RCC	6.877	70	6 584	10 303
	large-ANO-RCC	6.753	72	7 154	9 933
	ECP(MRCI) ³⁶	6.984	65	4 839	13 711
$1_u(^3\Sigma_u^+)$	TZ-ANO-RCC	7.681	55	3 618	13 155
	QZ-ANO-RCC	7.633	57	3 998	12 889
	large-ANO-RCC	7.566	61	4 837	12 249
	ECP(MRCI) ³⁶	7.544	54	2 662	15 244
$0_u^+(^3\Pi_u)$	TZ-ANO-RCC	8.927	17	500	16 272
	QZ-ANO-RCC	8.575	25	652	16 236
	large-ANO-RCC	8.450	32	977	16 109
	ECP(MRCI) ³⁶	8.714	26	484	18 067

Table 9: SO-CAS(4,8)PT2 adiabatic electronic states of Yb₂ dissociating into the $^1S+^3P_1$ atomic limit. r_e denotes the equilibrium bond length, ω_e the vibrational frequency, D_e the potential depth, and T_e the adiabatic excitation energy, respectively.

CONCLUSIONS AND OUTLOOK

In this work, we have investigated the electronic structure of atomic and molecular ytterbium using modern, state-of-the-art quantum chemistry methods. Our numerical analysis suggests that SO-CASPT2 with inclusion of the 5d orbitals into the active space can accurately reproduce the experimental energy levels of Yb. The singlet excited states in the Yb atom can be reliably modeled within the EOM-CCSD approach. A similar accuracy in excited state energies and properties can also be obtained with simplified alternatives, such as EOM-

State	basis	r_e [a ₀]	ω_e [cm ⁻¹]	D_e [cm ⁻¹]	T_e [cm ⁻¹]
$2_g(^3\Pi_g)$	TZ-ANO-RCC	6.964	69	6 303	11 651
	QZ-ANO-RCC	6.909	70	6 685	11 354
	large-ANO-RCC	6.814	72	7 605	10 632
	ECP(MRCI) ³⁶	6.998	66	5 565	14 437
$0_u^-(^3\Pi_u)$	TZ-ANO-RCC	8.626	29	1 403	16 552
	QZ-ANO-RCC	8.528	32	1 549	16 490
	large-ANO-RCC	8.490	32	1 786	16 450
	ECP(MRCI) ³⁶	8.404	31	1 452	18 551
$1_u(^3\Pi_u)$	TZ-ANO-RCC	8.820	23	902	17 052
	QZ-ANO-RCC	8.668	24	1 012	17 026
	large-ANO-RCC	8.368	30	1 284	16 952
	ECP(MRCI) ³⁶	8.596	27	1 049	18 954
$2_u(^3\Pi_u)$	TZ-ANO-RCC	8.931	19	382	17 572
	QZ-ANO-RCC	8.716	21	486	17 552
	large-ANO-RCC	8.342	29	755	17 482
	ECP(MRCI) ³⁶	8.755	27	484	19 519
$1_g(^1\Pi_g, ^3\Sigma_g^+)$	TZ-ANO-RCC	12.533	26	88	17 866
	QZ-ANO-RCC	11.160	18	81	17 957
	large-ANO-RCC	10.943	21	321	17 916
	ECP(MRCI) ³⁶	6.837	76	1 129	18 873

Table 10: SO-CAS(4,8)PT2 adiabatic electronic states of Yb₂ dissociating into the $^1S+^3P_2$ atomic limit. r_e denotes the equilibrium bond length, ω_e the vibrational frequency, D_e the potential depth, and T_e the adiabatic excitation energy, respectively.

pCCD-LCCSD.

Furthermore, we report a new set of spectroscopic parameters for the ground-state potential energy curve of the Yb₂ dimer. Our best estimate based on CCSD(T) reference calculations with an uncontracted ANO-RCC basis set gives an optimal bond length of

State	basis	r_e [a ₀]	ω_e [cm ⁻¹]	D_e [cm ⁻¹]	T_e [cm ⁻¹]
$0_u^+(^1\Sigma_u^+)$	TZ-ANO-RCC	7.173	81	9 089	19 194
	QZ-ANO-RCC	7.378	55	8 765	18 947
	large-ANO-RCC ^a	-	-	-	-
	ECP(MRCI) ³⁶	7.347	59	7 743	23 713
$1_u(^1\Pi_u)$	TZ-ANO-RCC	7.312	66	5 582	22 702
	QZ-ANO-RCC	7.272	67	5 484	22 228
	large-ANO-RCC	7.199	69	6 127	21 328
	ECP(MRCI) ³⁶	7.170	68	5 001	26 455
$0_g^+(^1\Sigma_g^+)$	TZ-ANO-RCC	7.505	65	5 041	23 243
	QZ-ANO-RCC	7.524	57	4 853	22 859
	large-ANO-RCC	7.666	55	5 011	22 444
	ECP(MRCI) ³⁶	7.514	51	3 549	27 907
$1_g(^3\Sigma_g^+, ^1\Pi_g)$	TZ-ANO-RCC	7.852	60	1 917	26 366
	QZ-ANO-RCC	7.802	64	2 200	25 512
	large-ANO-RCC	7.704	69	3 032	24 423
	ECP(MRCI) ³⁶	8.484	115	9 033	22 422

Table 11: SO-CAS(4,8)PT2 adiabatic electronic states of Yb₂ dissociating into the ¹S+¹P₁ atomic limit. r_e denotes the equilibrium bond length, ω_e the vibrational frequency, D_e the potential depth, and T_e the adiabatic excitation energy, respectively.

^a not computed due to technical difficulties

$r_e = 8.814$ bohr, a harmonic vibrational frequencies of $\omega_e = 21$ cm⁻¹, and a potential energy depth of $D_e = 579$ cm⁻¹ and can be considered as the limit of present-day quantum chemistry calculations. The CCSD potential energy curve, which results in an elongated bond length and underestimated potential energy depth compared to CCSD(T), can be reliably approximated using the pCCD-LCSSD and CAS(4,8)PT2 approaches.

The quantum chemical modeling of excited states in the Yb₂ dimer remains, however, a

remarkable challenge for present-day quantum chemistry. First, it is technically challenging to include d-type and f-type orbitals in molecular CASSCF calculations, limiting the manifold of electronic excitations to electron transfer from 6s to 6p atomic orbitals. Second, the $^1\Sigma_g^+$ excited state has a double excitation character that is difficult to describe using conventional coupled cluster type methods such as EOM-CCSD. The EOM-pCCD-LCCSD approach is advantageous here as it provides accurate spectroscopic constants, yet being able to correctly model the doubly excited $^1\Sigma^+$ potential energy curve. Most importantly, our numerical results indicate that the simplified EOM-pCCD-LCCSD formalism poses an alternative to the conventional EOM-CCSD approach to model excited states. Specifically, for most excited states, EOM-pCCD-LCCSD (with or without orbital optimization) provides spectroscopic constants that deviate less from the SO-CAS(4,8)PT2 reference values. This is especially advantageous for excited states with significant bi-excited character, where EOM-CCSD is known to fail.

Finally, we report a new set of reference spectroscopic constants for the low-lying excited states of the Yb_2 dimer using the SO-CAS(4,8)PT2 approach. Our data is a significant improvement over the existing ECP/SO-MRCI results of Wang and Dolg³⁶ as they include an all-electron basis set and a more rigorous treatment of scalar relativistic and electron correlation effects within the CASPT2 approach. Moreover, we investigate the convergence of the spectroscopic parameters (optimal bond lengths, vibrational frequencies, potential energy depths, and adiabatic excitation energies) with respect to the size of the basis set, which highlights the need for large basis set when modeling excited state potential energy curves in Yb_2 . We would like to stress that new quantum chemistry methods are desirable that can be used to reliably model the complete set of excited state potential energy curves in challenging molecules like the Yb_2 dimer.

High quality potential curves for the Yb_2 molecule are critical for future investigations in the fields of cold atomic collisions and ultracold molecules, including an improved description of the strengths and widths of intercombination line optical Feshbach resonances,^{12,86} searching for routes to Yb_2 rovibrational ground state,⁸⁷ or calculating the sensitivity of deeply bound molecular clock states to the variation of the proton-to-electron mass ratio^{21,30}. Finally, these potential curves provide a valuable starting point for laser-induced fluorescence

spectroscopy spectroscopy of ytterbium molecules.

ACKNOWLEDGMENTS

P.T. thanks a POLONEZ 1 research grant (no. 2015/19/P/ST4/02480) financed by Marie-Skłodowska-Curie COFUND. This project has received funding from the European Union's Horizon 2020 research and innovation programme under the Marie Skłodowska-Curie grant agreement No 665778. K.B. acknowledges financial support from a Marie-Skłodowska-Curie Individual Fellowship project no. 702635-PCCDX and a scholarship for outstanding young scientists from the Ministry of Science and Higher Education. M.B. and P.Sz.Ż. acknowledge financial support from the National Science Centre, Poland (no. 2017/25/B/ST4/01486). The research is part of an ongoing research program of the National Laboratory FAMO in Torun, Poland. D.K. acknowledges support from an OPUS grant of the National Science Centre, Poland (no. DEC-2012/07/B/ST4/01347) and COST Action CM1405 "Molecules in Motion" (MOLIM).

Calculations have been carried out using resources provided by Wrocław Centre for Networking and Supercomputing (<http://wcss.pl>), grant nos. 353, 411, and 412.

References

1. K. Honda, Y. Takasu, T. Kuwamoto, M. Kumakura, Y. Takahashi, and T. Yabuzaki, *Phys. Rev. A* **66**, 021401 (2002).
2. M. Kitagawa, K. Enomoto, K. Kasa, Y. Takahashi, R. Ciuryło, P. Naidon, and P. S. Julienne, *Phys. Rev. A* **77**, 012719 (2008).
3. Y. Takasu, K. Maki, K. Komori, T. Takano, K. Honda, M. Kumakura, T. Yabuzaki, and Y. Takahashi, *Phys. Rev. Lett.* **91**, 040404 (2003).
4. T. Fukuhara, S. Sugawa, and Y. Takahashi, *Phys. Rev. A* **76**, 051604(R) (2007).
5. T. Fukuhara, S. Sugawa, Y. Takasu, and Y. Takahashi, *Phys. Rev. A* **79**, 021601(R) (2009).
6. S. Sugawa, R. Yamazaki, S. Taie, and Y. Takahashi, *Phys. Rev. A* **84**, 011610(R) (2011).
7. A. D. Ludlow, M. M. Boyd, J. Ye, E. Peik, and P. O. Schmidt, *Rev. Mod. Phys.* **87**, 638 (2015).
8. W. F. McGrew, X. Zhang, R. J. Fasano, S. A. Schäffer, K. Beloy, D. Nicolodi, R. C. Brown, N. Hinkley, G. Milani, M. Schioppo, et al., *Nature* **564**, 87 (2018).
9. L. F. Livi, G. Cappellini, M. Diem, L. Franchi, C. Clivati, M. Frittelli, F. Levi, D. Calonico, J. Catani, M. Inguscio, et al., *Phys. Rev. Lett.* **117**, 1 (2016).
10. K. M. Jones, E. Tiesinga, P. D. Lett, and P. S. Julienne, *Rev. Mod. Phys.* **78**, 483 (2006).
11. S. Tojo, M. Kitagawa, K. Enomoto, Y. Kato, Y. Takasu, M. Kumakura, and Y. Takahashi, *Phys. Rev. Lett.* **96**, 153201 (2006).
12. M. Borkowski, R. Ciuryło, P. S. Julienne, S. Tojo, K. Enomoto, and Y. Takahashi, *Phys. Rev. A* **80**, 012715 (2009).
13. M. Borkowski, A. A. Buchachenko, R. Ciuryło, P. S. Julienne, H. Yamada, Y. Kikuchi, K. Takahashi, Y. Takasu, and Y. Takahashi, *Phys. Rev. A* **96**, 063405 (2017).

14. Y. Takasu, Y. Saito, Y. Takahashi, M. Borkowski, R. Ciuryło, and P. S. Julienne, Phys. Rev. Lett. **108**, 173002 (2012).
15. K. Enomoto, M. Kitagawa, S. Tojo, and Y. Takahashi, Phys. Rev. Lett. **100**, 123001 (2008).
16. R. Ciuryło, E. Tiesinga, and P. S. Julienne, Phys. Rev. A **71**, 030701(R) (2005).
17. K. Enomoto, K. Kasa, M. Kitagawa, and Y. Takahashi, Phys. Rev. Lett. **101**, 203201 (2008).
18. M.-S. Kim, J. Lee, J. H. Lee, Y. Shin, and J. Mun, Phys. Rev. A **94**, 042703 (2016).
19. L. Franchi, L. F. Livi, G. Cappellini, G. Binella, M. Inguscio, J. Catani, and L. Fallani, New J. Phys **19**, 103037 (2017).
20. R. Bouganne, M. B. Aguilera, A. Dureau, E. Soave, J. Beugnon, and F. Gerbier, New J. Phys. **19**, 113006 (2017).
21. M. Borkowski, Phys. Rev. Lett. **120**, 083202 (2018).
22. G. Pagano, M. Mancini, G. Cappellini, L. Livi, C. Sias, J. Catani, M. Inguscio, and L. Fallani, Phys. Rev. Lett. **115** (2015).
23. G. Cappellini, L. F. Livi, L. Franchi, D. Tusi, D. Benedicto Orenes, M. Inguscio, J. Catani, and L. Fallani, Phys. Rev. X **9**, 011028 (2019).
24. S. Kato, S. Sugawa, K. Shibata, R. Yamamoto, and Y. Takahashi, Phys. Rev. Lett. **110**, 173201 (2013).
25. Y. Takasu, Y. Fukushima, Y. Nakamura, and Y. Takahashi, Phys. Rev. A **96**, 023602 (2017).
26. D. G. Green, C. L. Vaillant, M. D. Frye, M. Morita, and J. M. Hutson, Phys. Rev. A **93**, 022703 (2016).
27. M. S. Safronova, S. G. Porsev, C. Sanner, and J. Ye, Phys. Rev. Lett. **120**, 173001 (2018).

28. E. R. Meyer and J. L. Bohn, *Phys. Rev. A* **80**, 042508 (2009).
29. M. Borkowski, A. A. Buchachenko, R. Ciuryło, P. S. Julienne, H. Yamada, Y. Kikuchi, Y. Takasu, and Y. Takahashi (2018), 1612.03842, URL <http://arxiv.org/abs/1612.03842>.
30. T. Zelevinsky, S. Kotochigova, and J. Ye, *Phys. Rev. Lett.* **100**, 043201 (2008).
31. T. Takekoshi, L. Reichsöllner, A. Schindewolf, J. M. Hutson, C. R. Le Sueur, O. Dulieu, F. Ferlaino, R. Grimm, and H. C. Nägerl, *Phys. Rev. Lett.* **113**, 1 (2014).
32. T. Fleig, *Chem. Phys.* **395**, 2 (2011).
33. A. A. Buchachenko, G. Chałasiński, and M. M. Szczyński, *Eur. Phys. J. D* **45**, 147 (2007).
34. M. S. Safronova, S. G. Porsev, and C. W. Clark, *Phys. Rev. Lett.* **109**, 230802 (2012).
35. S. G. Porsev, M. S. Safronova, A. Derevianko, and C. W. Clark, *Phys. Rev. A* **89**, 012711 (2014).
36. Y. Wang and M. Dolg, *Theor. Chem. Acc.* **100**, 124 (1998).
37. B. O. Roos, R. Lindh, P.-A. Malmqvist, V. Veryazov, P.-O. Widmark, and A. C. Borin, *J. Phys. Chem. A* **112**, 11431 (2008).
38. N. Douglas and N. M. Kroll, *Ann. Phys.* **82**, 89 (1974).
39. B. A. Hess, *Phys. Rev. A* **33**, 3742 (1986).
40. P. A. Johnson, P. W. Ayers, P. A. Limacher, S. de Baerdemacker, D. van Neck, and P. Bultinck, *J. Chem. Theor. Comput.* **1003**, 101 (2013).
41. T. Stein, T. M. Henderson, and G. E. Scuseria, *J. Chem. Phys.* **140**, 214113 (2014).
42. PIERNIK, a pythonic ab initio electronic structure program, (2019), written by F. Brzęk, A. Leszczyk, A. Nowak, K. Boguslawski, D. Kędziera, P. Tecmer, and P. S. Żuchowski.

43. K. Boguslawski, P. Tecmer, P. W. Ayers, P. Bultinck, S. De Baerdemacker, and D. Van Neck, *Phys. Rev. B* **89**, 201106(R) (2014).
44. K. Boguslawski, P. Tecmer, P. A. Limacher, P. A. Johnson, P. W. Ayers, P. Bultinck, S. De Baerdemacker, and D. Van Neck, *J. Chem. Phys.* **140**, 214114 (2014).
45. K. Boguslawski, P. Tecmer, P. W. Ayers, P. Bultinck, S. De Baerdemacker, and D. Van Neck, *J. Chem. Theory Comput.* **10**, 4873 (2014).
46. K. Boguslawski and P. W. Ayers, *J. Chem. Theory Comput.* **11**, 5252 (2015).
47. K. Boguslawski, *J. Chem. Phys.* **145**, 234105 (2016).
48. K. Boguslawski, *J. Chem. Phys.* **147**, 139901 (2017).
49. K. Boguslawski, *J. Chem. Theory Comput.* **15**, 18 (2019).
50. A. Leszczyk, P. Tecmer, and K. Boguslawski, in *Transition Metals in Coordination Environments, Challenges and Advances in Computational Chemistry and Physics* (Springer, Cham (Switzerland), 2019), vol. 29, chap. New Strategies in Modeling Electronic Structures and Properties with Applications to Actinides, pp. 121–160.
51. M. J. O. Deegan and P. J. Knowles, *Chem. Phys. Lett.* **227**, 321 (1994).
52. T. Korona and H.-J. Werner, *J. Chem. Phys.* **118**, 3006 (2003).
53. H. Werner, P. J. Knowles, G. Knizia, F. R. Manby, M. Schütz, and et al., *Molpro, version 2012.1, a package of ab initio programs* (2012), see <http://www.molpro.net>.
54. H. Werner, P. J. Knowles, G. Knizia, F. R. Manby, and M. Schütz, *WIREs Comput. Mol. Sci.* **2**, 242 (2012).
55. H. Werner and P. J. Knowles, *J. Chem. Phys.* **82**, 5053 (1985).
56. H. Werner and P. J. Knowles, *J. Chem. Phys.* **89**, 5803 (1988).
57. B. O. Roos, P. R. Taylor, and P. E. M. Siegbahn, *Chem. Phys.* **48**, 157 (1980).

58. P. E. M. Siegbahn, J. Almlöf, A. Heiberg, and B. O. Roos, *J. Chem. Phys.* **74**, 2384 (1981).
59. K. Andersson, P.-Å. Malmqvist, B. O. Roos, A. J. Sadlej, and K. Woliński, *J. Phys. Chem.* **94**, 5483 (1990).
60. K. Andersson, P.-Å. Malmqvist, and B. O. Roos, *J. Chem. Phys.* **96**, 1218 (1992).
61. J. Finley, P.-Å. Malmqvist, B. O. Roos, and L. Serrano-Andrés, *Chem. Phys. Lett.* **288**, 299 (1998).
62. G. Karlström, R. Lindh, P.-Å. Malmqvist, B. O. Roos, U. Ryde, V. Veryazov, P.-O. Widmark, M. Cossi, B. Schimmelpfennig, P. Neogrády and L. Seijo, *Comput. Mater. Sci.* **28**, 222 (2003).
63. F. Aquilante, L. De Vico, N. Ferré, G. Ghigo, P.-Å. Malmqvist, P. Neogrády, T. B. Pedersen, M. Pitonak, M. Reiher, B. O. Roos, L. Serrano-Andrés, M. Urban, V. Veryazov and R. Lindh, *J. Comput. Chem.* **31**, 224 (2010).
64. V. Veryazov, P.-O. Widmark, L. Serrano-Andrés, R. Lindh and B. O. Roos, *Int. J. Quantum Chem.* **100**, 626 (2004).
65. F. Aquilante, J. Autschbach, R. K. Carlson, L. F. Chibotaru, M. G. Delcey, L. De Vico, I. Fdez. Galván, N. Ferré, L. M. Frutos, L. Gagliardi, M. Garavelli, A. Giussani, C. E. Hoyer *et al.*, *J. Comput. Chem.* **37**, 506 (2016).
66. G. Ghigo, B. O. Roos, and P.-Å. Malmqvist, *Chem. Phys. Lett.* **396**, 142 (2004).
67. B. A. Hess, C. M. Marian, U. Wahlgren, and O. Gropen, *Chem. Phys. Lett.* **251**, 365 (1996).
68. C. M. Marian and U. Wahlgren, *Chem. Phys. Lett.* **251**, 357 (1996).
69. B. Schimmelpfennig, L. Maron, U. Wahlgren, C. Teichtel, H. Fagerli, and O. Gropen, *Chem. Phys. Lett.* **286**, 267 (1998).

70. P.-Å. Malmqvist, B. O. Roos, and B. Schimmelpfennig, *Chem. Phys. Lett.* **357**, 230 (2002).
71. M. Abramowitz and I. A. Stegun, *Handbook Of Mathematical Functions With Formulas, Graphs, And Mathematical Tables* (Dover, New York, 1970).
72. J. E. Sansonetti and W. C. Martin, *J. Phys. Chem. Ref. Data* **34**, 1559 (2005).
73. W. F. Meggers and J. L. Tech, *J. Res. Natl. Bur. Stand. U.S.* **83**, 13 (1978).
74. F. Mies, W. Stevens, and M. Krauss, *J. Mol. Spectrosc.* **72**, 303 (1978).
75. B. O. Roos, in *Radiation Induced Molecular Phenomena in Nucleic Acids* (Springer, 2008), pp. 125–156.
76. S. Suzer and L. Andrews, *J. Chem. Phys.* **89**, 5514 (1988).
77. Y. Wang, F. Schautz, H.-J. Flad, and M. Dolg, *J. Phys. Chem. A* **103**, 5091 (1999).
78. J. Řezáč and P. Hobza, *J. Chem. Theory Comput.* **9**, 2151 (2013).
79. S. Boys and F. Bernardi, *Mol. Phys.* **19**, 553 (1970).
80. P. Goodfriend, *Spectrochim. Acta A: Mol. Spectr.* **40**, 283 (1984).
81. T. J. Lee and P. R. Taylor, *Int. J. Quantum Chem.* **23**, 199 (1989).
82. N. S. Mosyagin, P. A. N., and A. Titov, pp. 1–10 (2009), 0901.0077v6.
83. K. Boguslawski, P. Tecmer, P. A. Limacher, P. A. Johnson, P. W. Ayers, P. Bultinck, S. de Baerdemacker, and D. van Neck, *J. Chem. Phys.* **140**, 214114 (2014).
84. K. Boguslawski, P. Tecmer, P. A. Limacher, P. A. Johnson, P. W. Ayers, P. Bultinck, S. de Baerdemacker, and D. van Neck, *J. Chem. Theory Comput.* **10**, 4873 (2014).
85. T. Helgaker, W. Klopper, H. Koch, and J. Noga, *J. Chem. Phys.* **106**, 9639 (1997).
86. T. L. Nicholson, S. Blatt, B. J. Bloom, J. R. Williams, J. W. Thomsen, J. Ye, and P. S. Julienne, *Phys. Rev. A* **92**, 022709 (2015).

87. J. M. Sage, S. Sainis, T. Bergeman, and D. DeMille, *Phys. Rev. Lett.* **94**, 203001 (2005).